Analysis of experimental data: The average shape of extreme wave forces on monopile foundations and the NewForce model

Schløer, Signe; Bredmose, Henrik; Ghadirian, Amin

Published in:
Energy Procedia

Link to article, DOI:
10.1016/j.egypro.2017.10.376

Publication date:
2017

Document Version
Publisher's PDF, also known as Version of record

Available online at www.sciencedirect.com

ScienceDirect

Energy Procedia 137 (2017) 223–237

Energy Procedia

www.elsevier.com/locate/procedia

14th Deep Sea Offshore Wind R&D Conference, EERA DeepWind'2017, 18-20 January 2017, Trondheim, Norway

Analysis of experimental data: The average shape of extreme wave forces on monopile foundations and the NewForce model

Signe Schløer[a,*], Henrik Bredmose[a], Amin Ghadirian[a]

[a]*DTU Wind Energy, Nils Koppels Alle, Building 403, DK-2800 Kgs. Lyngby, Denmark*

Abstract

Experiments with a stiff pile subjected to extreme wave forces typical of offshore wind farm storm conditions are considered. The exceedance probability curves of the nondimensional force peaks and crest heights are analysed. The average force time history normalised with their peak values are compared across the sea states. It is found that the force shapes show a clear similarity when grouped after the values of the normalised peak force, $F/(\rho g h R^2)$, normalised depth $h/(gT_p^2)$ and presented in a normalised time scale t/T_a. For the largest force events, slamming can be seen as a distinct 'hat' on top of the smoother underlying force curve.

The force shapes are numerically reproduced using a design force model, NewForce, which is introduced here for the first time to both first and second order in wave steepness. For force shapes which are not asymmetric, the NewForce model compares well to the average shapes. For more nonlinear wave shapes, higher order terms has to be considered in order for the NewForce model to be able to predict the expected shapes.

Peer-review under responsibility of SINTEF Energi AS.

Keywords: NewForce; Experimental data; Average force shape; Extreme forces

1. Introduction

In today's design of offshore wind turbines, the extreme waves are based on probability distributions from measurements and hindcast models. In the dynamic analysis, the extreme waves are often calculated by stream function wave theory embedded into a linear irregular time series. The wave period of the stream function wave should according to [9] be the period inside a predefined interval as function of the wave height, which gives the largest load. The wave force is typically calculated by Morison's equation. Instead of stream function waves, NewWave theory, [1,11,17], can also be used to calculate the extreme waves. The NewWave is a deterministic design wave, where the crest amplitude is predefined and the time history of the crest is described by the autocorrelation function of the wave spectrum, assuming the surface elevation to be a linear random Gaussian process.

The NewWave has been validated to experimental data and real measurements in a number of studies, cf. [3,8, 15,18,19]. Whittaker et al., [19], showed that NewWave theory compares well to the linearised average shape of the

* Corresponding author. Tel.: +0-000-000-0000 ; fax: +0-000-000-0000.
E-mail address: sigs@dtu.dk

1876-6102
Peer-review under responsibility of SINTEF Energi AS.
10.1016/j.egypro.2017.10.376

largest waves during a storm for nondimensional wave numbers down to $kh = 0.4$, with k being the wave number and h the water depth. Further, a second-order corrected NewWave profile compared resonable to the average measured wave profile.

However, as will be shown in this paper, it is not always the wave with the largest wave height or crest height, which results in the largest wave force. Instead, the largest force could be due to a wave with a smaller wave height and amplitude but with a very steep wave crest. Less uncertainty on the extreme wave force would thus be obtained if based on probability distributions of the force itself instead of wave height.

For nonlinear regular waves, Paulsen et al. [12] found a similarity in the temporal development of the normalised force time histories, F/F_{max} as function of H/H_{max}, where H is the wave height and H_{max} is the maximum wave height at the given nondimensional depth from the wave breaking criterion of [20]. Further, the force peak value, $F_{max}/(\rho g h R^2)$ was found to increase with H/H_{max} but was independent of the nondimenisonal water depth kh. Here ρ is the density of water, g the gravity and R the radius of the monopile.

In the present paper it is investigated if a similar correlation can be found for experimental measured extreme response forces on a monopile foundation from irregular waves, and whether these forces can be predicted numerically if only information about the water depths, the significant wave heights, H_s and peak wave periods, T_p, of the wave realizations are known. To do this the NewForce model is introduced here for the first time. It can be seen as a design force in same way as the NewWave theory for the free surface elevation. The model is compared to second order FORM analysis in [6].

The paper opens with an outset of the analysis and a presentation of the NewForce model. Next the model test considered in the analysis are introduced and exceedance probability curves of the nondimensional crest heights of the free surface elevation and force peaks are presented for the different sea states. Based on the probability curves, the forces shapes conditional to a given normalised force peak level are compared across a the different sea states and a relation between the shapes are found. The force shapes are further compared to the NewForce model. The paper ends with a summary and discussion.

2. Outset of the analysis

In Offshore Engineering, design wave loads are often derived with basis in a certain design wave height and subsequent application of a wave theory and a force model. However, as the peak force is not just a function of wave height but also depends on e.g. the wave front slope, the resulting design load is associated with uncertainty. Some of this uncertainty can be by-passed if the force statistics of the given structure is known. In that case, the design loads for a static design are readily available. However, in order to run dynamic calculations, information about the force variation in space and time is also necessary. The present paper seeks to provide these two pieces of information by analysis of experimental measurements on a monopile. We will use the word shape as an alternative denotation of time history throughout.

Consider a monopile of radius R at depth h, subjected to a JONSWAP sea state with significant wave height H_s, peak period T_p and peak enhancement factor γ. We further denote the water density by ρ, gravity by g and the water viscosity by ν. A given realization of the sea state can be characterized by a set of stochastic variables $\{x_j\}$, and for such a realization the force time series can be expressed by

$$\frac{F}{\rho g h R^2} = f\left(\frac{H_s}{gT_p^2}, \frac{h}{gT_p^2}, \gamma, \frac{R}{gT_p^2}, \frac{\nu}{\sqrt{ghR^2}}, \frac{t}{T_p}, \{x_j\}\right). \tag{1}$$

The force peaks may be sorted in increasing order to estimate the associated probability distribution, which may be expressed as a function of the same parameters

$$P\left(\frac{F_i}{\rho g h R^2} \le \frac{F}{\rho g h R^2}\right) = f_1\left(\frac{F_i}{\rho g h R^2}, \frac{H_s}{gT_p^2}, \frac{h}{gT_p^2}, \gamma, \frac{R}{gT_p^2}, \frac{\nu}{\sqrt{ghR^2}}\right), \tag{2}$$

where the time and stochastic variables $\{x_j\}$ are now removed.

For a given value of F_i, the expected force history can be determined by ensemble averaging. This expected time history can thus be expressed by

$$\frac{F}{F_i} = f_2\left(\frac{F_i}{\rho g h R^2}, \frac{H_s}{gT_p^2}, \frac{h}{gT_p^2}, \gamma, \frac{R}{gT_p^2}, \frac{\nu}{\sqrt{ghR^2}}, \frac{t}{T_p}\right). \tag{3}$$

In the present paper we estimate the shape of f_1 and f_2 based on an experimental data set from the DeRisk project [2]. The data set covers a limited parameter set relevant for offshore wind turbine monopiles in storm conditions, and we therefore reduce the parameter space accordingly. First, the peak enhancement parameter γ is expressed as a function of H_s and T_p (see [9]). Next, since the tests were carried out with a fixed pile diameter, the influence of R/gT_p^2 is neglected. Since the sea states studied are all storm sea states, all the wave episodes considered are to good approximation in the long wave regime. Further, the Reynolds number dependence through ν is ignored along with any other scale effects from e.g. aeration. This leads to the simplified dependencies

$$P\left(\frac{F_i}{\rho g H_s R^2} \le \frac{F}{\rho g H_s R^2}\right) = f_1\left(\frac{F_i}{\rho g h R^2}, \frac{H_s}{gT_p^2}, \frac{h}{gT_p^2}\right) \tag{4}$$

$$\frac{F}{F_i} = f_2\left(\frac{F_i}{\rho g h R^2}, \frac{H_s}{gT_p^2}, \frac{h}{gT_p^2}, \frac{t}{T_a}\right). \tag{5}$$

Here, the functional dependencies have further been modified such that the force levels are normalized with H_s instead of h in the denominator to accommodate the expected linear behaviour and where time in f_2 is normalized with a new time scale T_a, which will be defined later in terms of γ and T_p. The role of the present work is thus to investigate the functional dependencies of (f_1, f_2) to the wave parameters by analysis of experimental results. Further, the shape of f_2 is compared to the NewForce signal to investigate how well the NewForce model can reproduce the shape.

3. The NewForce model

The NewWave theory was derived by [1,11,17]. Given a power spectrum of free surface elevation S_η, the NewWave theory establishes the expected time history of free surface elevation around a peak as

$$\eta_{\text{NewWave}} = \frac{\alpha_\eta}{\sigma_\eta^2} \sum_j \text{Re}\left\{S_\eta(\omega_j)\Delta\omega \exp\left(\text{i}\left(\omega_j(t-t_0) - k_j(x-x_0)\right)\right)\right\}, \tag{6}$$

where α_η is the crest height and $\sigma_\eta^2 = \overline{\eta^2} = \int_{\omega=0}^{\infty} S_\eta(\omega)\,\text{d}\omega$. It is thus a linear theory and the associated linear force history can be derived through its linear transfer function. Assuming that the wave force is inertia-dominated, thus neglecting the drag-contribution, this transfer function can be obtained through the Morison equation

$$\Gamma(\omega) = \text{i}\rho\pi R^2 C_M \omega^2/k \tag{7}$$

and involves a phase shift of $\pi/2$ through the i-factor. Further, C_M is the inertia coefficient and k the wave number.

The inline force for the NewWave free surface history (6) is thus

$$F_{\text{NewWave}} = \frac{\alpha_\eta}{\sigma_\eta^2} \sum_j \text{Re}\left\{S_\eta(\omega_j)\Gamma(\omega)\Delta\omega \exp\left(\text{i}\left(\omega_j(t-t_0) - k_j(x-x_0)\right)\right)\right\}. \tag{8}$$

The NewForce model takes basis in the linear force spectrum $S_F(\omega) = |\Gamma(\omega)|^2 S_\eta(\omega)$. We re-apply the principle of NewWave to obtain the expected force history around a force peak from the linear force spectrum:

$$F^{(1)}_{\text{NewForce}} = \frac{\alpha_F}{\sigma_F^2} \sum_j \text{Re}\left\{\left|\Gamma(\omega_j)\right|^2 S_\eta(\omega_j)\Delta\omega \exp\left(\text{i}\left(\omega_j(t-t_0) - k_j(x-x_0)\right)\right)\right\}. \tag{9}$$

Here α_F is the force peak value and σ_F^2 is the integrated force spectrum. Due to its linear origin, the NewForce signal is symmetric around the peak. The associated time history of the free surface elevation is obtained by division with the force transfer function $\Gamma(\omega)$ as

$$\eta^{(1)}_{\text{NewForce}} = \frac{\alpha_F}{\sigma_F^2} \sum_j \text{Re}\left\{\Gamma^*(\omega_j) S_\eta(\omega_j) \Delta\omega \exp\left(\text{i}\left(\omega_j(t-t_0) - k_j(x-x_0)\right)\right)\right\}, \tag{10}$$

where Γ^* is the complex conjugate of Γ.

We note that the free surface elevation history associated with the NewForce model differs from the classical NewWave theory by a phase shift of $\pi/2$ of all the wave components and multiplication by the linear force transfer function inside the sum. The wave time history that produces a given force with largest probability is thus different from a simple phase shift of $\pi/2$ of the classical NewWave signal. The NewForce signal principle can readily be applied to other quantities of interest such as e.g. overturning moment as long as this can be expressed through a linear transfer function applied to the free surface elevation signal.

The NewForce signal is only first-order accurate, but the second order contribution can easily be added by 1) calculation of the second-order components of the incident wave field and kinematics by the the second order wave theory of [16] and 2) by adding the second-order contributions from the slender-body force model that goes beyond linear theory. In the analysis it is decided only to use Morison equation up to second order to be consistent with the used wave theory

$$\begin{aligned} F^{(2)}_{\text{NewForce}} =& \rho\pi R^2 C_M \int_{-h}^{0} (u_t^{(2)} + u^{(1)}u_x^{(1)} + w^{(1)}u_z^{(1)})\text{d}z + \rho R C_D \int_{-h}^{0} u^{(1)}|u^{(1)}|\text{d}z \\ &+ \rho\pi R^2 (C_M - 1) \int_{-h}^{0} (u^{(1)} w_z^{(1)})\text{d}z + \rho\pi R^2 C_M \eta^{(1)}_{NF} u_t^{(1)}. \end{aligned} \tag{11}$$

One reason for this, besides mathematical strictness, is that we will apply fully nonlinear wave kinematics in future work and therefore wish to work with a strictly linear, strictly second-order and fully nonlinear model. In (11) u and w are the horizontal and vertical particle velocities and $u_t = \frac{\partial u}{\partial t}$ the horizontal acceleration. Subscripts x and z means that the variables are differentiated with respect to these coordinates. The nonlinear Rainey terms, [13]-[14], are also included to second order in (11), third term. For the drag and inertia coefficients the generic values $C_D = 1$ and $C_M = 2$ have been used troughout. It should be noted that while the first-order NewForce (and NewWave) models is the most likely realization of a linear event of given peak amplitude, the second-order versions constructed by simple add-on of the second-order tems differ slightly from the most likely second-order event. For free surface elevation [10] derives expressions for the most likely second-order events while [6] calculate the most likely second-order force and free surface events by a first-order reliability method.

4. The model tests

The model tests were conducted at DHI Denmark, as part of the DeRisk-project (2015-2019, [2]). The domain was 18x20m and both uni-and multidirectional wave realizations based on JONSWAP-spectra were considered. The experiment was Froude-scaled with a scaling factor of 1:50.

Two water depths of $h = 0.66$m and $h = 0.4$m, 33 m and 20 m in full scale, with a flat sea bed were considered. The stiff pile had a diameter of $D = 0.14$m, 7 m in full scale, and was fixed at the bed and top. In the following, if nothing else is stated, all data are given in full scale. The scale effects of the model tests which exist for the impact pressures, impact forces and viscous loads are therefore omitted in the present study. However, for inertia dominated impacts, the scale effects are usually considered small.

The free surface elevations considered in the analysis were measured 0.1m (lab scale) in front of the pile. Both the forces in the inline and transverse wave direction were measured by force transducers, however in this analysis only the inline force is considered.

The force transducers were excited when large waves hit the structure. To ensure that this excitation is not part of the analysed force-signal, the excitation was filtered out using a low pass filter. Considering the force spectrum of figure 1 the spectrum contains energy around 0.1 Hz due to the wave signal but the signal also contains peaks for frequencies larger than 3 Hz, which is much higher than the wave frequencies. Frequencies higher than 2.5 Hz are therefore disregarded in the analysis. Also in figure 1, a force signal before and after the filtering is seen. It is easy to see that the force is smoothened after the filtering, but it is also seen that the slamming force (the peak of the force at time $t \sim 7760$s) is maintained.

4.1. The sea states

In the present paper only the uni-directional waves are analyzed. Five sea states on a water depth of 33 m and six sea states on a water depth of 20 m are considered. The lengths of the time series are 6 hours. The sea states are presented in table 1, where the significant wave height, peak wave period and water depth are listed. Figure 2 from [4] shows the steepness of the waves $H/(gT^2)$ as function of the nondimensional water depth $h/(gT^2)$. The larger $H/(gT^2)$, the more steep the waves of the sea state. Similarly, smaller values of $h/(gT^2)$, corresponds to more shallow depth conditions. For the considered sea states the steepness and nondimensional water depths are based on the significant wave height, H_s and peak wave period, T_p, also stated in the figure.

It is clear that none of the sea states can be described accurately with linear wave theory. Further the sea states are grouped after their $h/(gT_p^2)$-value, indicated with black circles. Three groups are defined with the average values $h/(gT_p^2) = 0.9\,, 0.014$ and 0.024. The color of each sea state is repeated through out the paper.

Table 1: Significant wave height, peak wave period and water depth of the considered wave realizations.

Test	H_s (m)	T_p (s)	h (m)
9	7.5	12	33
10	7.5	15	33
11	9.5	12	33
12	9.5	15.	33
13	11.0	15	33
20	5.8	12	20
21	5.8	15	20
22	6.8	12	20
23	6.8	15	20
24	7.5	15	20
25	5.8	9	20

5. Results

5.1. Exceedance probability distributions of the free surface elevation and force signals

In the following the functional dependencies of f_1 and f_2, (4)-(5), are investigated. In figure 3 the exceedance probability curves of the crest height and force peaks for all wave realizations are shown. The crest heights and force peaks are the largest value in between two neighbouring zero-down-crossings of the free surface elevations, which are sorted in increasing order. The probability of exceedance is here calculated as

$$P = 1 - \tfrac{i-1}{N}, \quad i = 1, 2, 3, ..., N, \tag{12}$$

where N is the number of waves in the time series. The crest heights and the force peaks are nondimenionalised as η/H_S and $F/(\rho g H_s R^2)$.

The curves in figure 3 are not fully identical. As the probability of exceedance decreases the difference between the curves increases. Furthermore, the relative difference between the smallest and largest crest height for the lowest exceedance probability is smaller than the difference between the smallest and largest force peaks. Thus, the expected

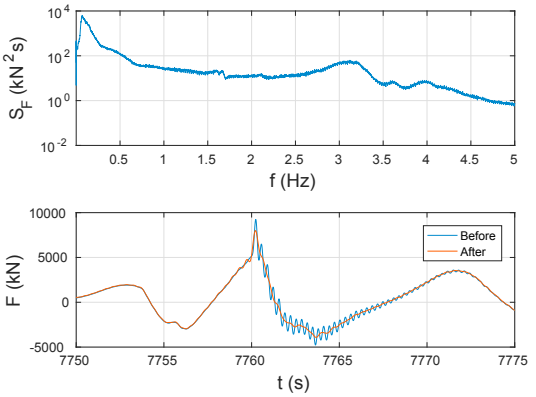

Fig. 1: The power spectrum and the time series of the measured force signal in full scale. Frequencies above 2.4 Hz are filtered out in the force-signal.

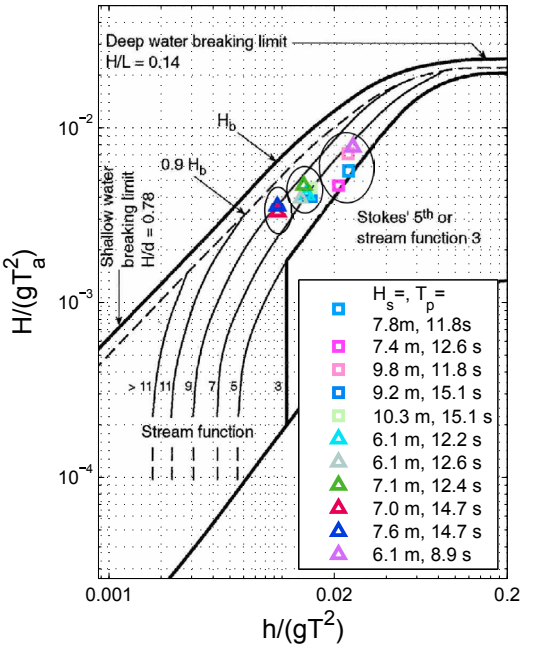

Fig. 2: Figure from [4] used to classify the sea states, based on H_s and T_p. □ h = 33m, △ h = 20m. The black circles indicate the three groups the sea states are divided into as function of $h/(gT_p^2)$.

linear behaviour of the crest heights and force peaks being proportional to the wave height does not hold for these sea states.

This means that the waves, as expected, are nonlinear and that their dependence to $h/(gT_p^2)$ cannot be ignored. For the further analysis, we therefore change the normalisation to $F/(\rho g h R^2)$ and η/h to make it independent of H_s. This way, events of same wave height or force level can be picked from sea states of different significant wave height and be compared. The associated exceedance probability curves are shown in figure 4. The difference between the curves are larger relative to figure 3 where the linear force dependence to H_s was included in the normalization.

The closer the sea states are to the wave breaking limit, cf. figure 2, the larger the force-peaks are for same probability value since the shape of the surface elevations become more steep the closer the waves are to breaking resulting in larger forces.

For some of the exceedance probability curves of the crest heights the tangents of the curves for the smallest probabilities is almost vertical, for example the sea state with H_s = 7.1m and T_p = 12.4s. If the largest crest height is left out of account, the values of the five second largest crest heights are almost identical. It could look like a breaking limit for which the crest height can not be larger. Comparing the time series of the force and free surface elevation, the force peaks corresponding to the largest five crest heights η/h are represented within the eight largest force values, $F/(g\rho h R^2)$. This indicates that the waves are or are close to breaking and that the forces are due to wave slamming.

As shown in (4) the probability distributions are functions of $H_s/(gT_p^2)$ and $h/(gT_p^2)$ but the ordering in magnitude is not coinciding. To illustrate this, nine peaks nearest different force values $F/(\rho g h R^2)$ are considered for all sea states in figure 5. Nine force peaks nearest $F/(\rho g h R^2)$ = 1.0 and $F/(\rho g h R^2)$ = 1.3 are indicated with red and black asterisks, respectively. In the figure the corresponding crest heights for the same waves are also indicated with red and black asterisks. It is seen that there is large variation in these crest values, but also there is a tendency that that the variation is smaller for the sea states where the considered force values, $F/(\rho g h R^2)$ = 1.0 and $F/(\rho g h R^2)$ = 1.3, are near the extreme force values. This could indicate that for the extreme forces of a sea state, the number of shapes which can result in these forces are reduced. In figure 6 the relation between the wave height and period of the waves resulting in these peaks are compared to the breaking criteria of [7]

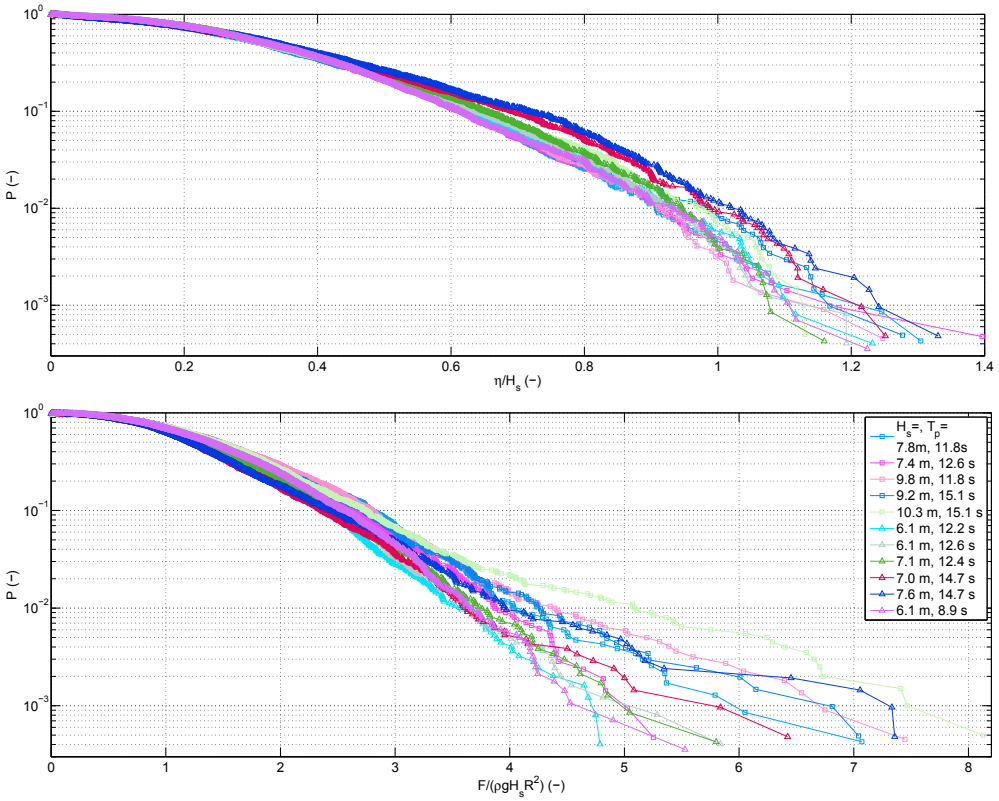

Fig. 3: Probability of exceedance of the crest heights and force peaks, when normalizing with H_S. □ h = 33m, △ h = 20m.

$$\frac{H_b}{L_0} = A\left(1 - \exp\left(-1.5\pi\frac{h}{L_0}\right)\right). \tag{13}$$

Here L_0 is the deep water wave length and H_b the limiting wave height. For irregular waves breaking occur for $0.12 < A < 0.18$. For linear waves, $L_0 = gT^2/(2\pi)$ and the nondimensional values $\frac{H_b}{L_0}$ and $\frac{h}{L_0}$ therefore correspond to the nondimensional values $\frac{H}{(gT^2)}$ and $\frac{h}{(gT^2)}$ on figure 2. A trend between the force values and the wave heights is seen. All the waves lie on a curve almost parallel to the breaking limits, and as the force value $F/(g\rho hR^2)$ increases, the waves are closer to breaking.

5.2. The averaged force shape

In the following it is investigated if a similarity of the force shapes with same force value $F/(\rho ghR^2)$ but different exceedance probability can be found. Irregular wave realizations are a stochastic process. In previous studies, where the NewWave is compared to extreme wave events in measured and calculated wave realizations, [8]-[19], the extreme waves are the average of a given number of the waves with largest crest height in the wave realization. The same approach is used in the present analysis, but on different levels of crest heights and force peak values.

In figure 7, the nine force shapes of the nine force peaks nearest $F/(\rho ghR^2) = 1.0$ and $F/(\rho ghR^2) = 1.3$ are shown for the sea state with $H_s = 10.3$ m, $T_p = 15.1$ s and $h = 33$ m together with the average force time series, F_A. The force peaks are centered at time $t = 0$ s. Before averaging the force shapes the forces are normalised with their peak values.

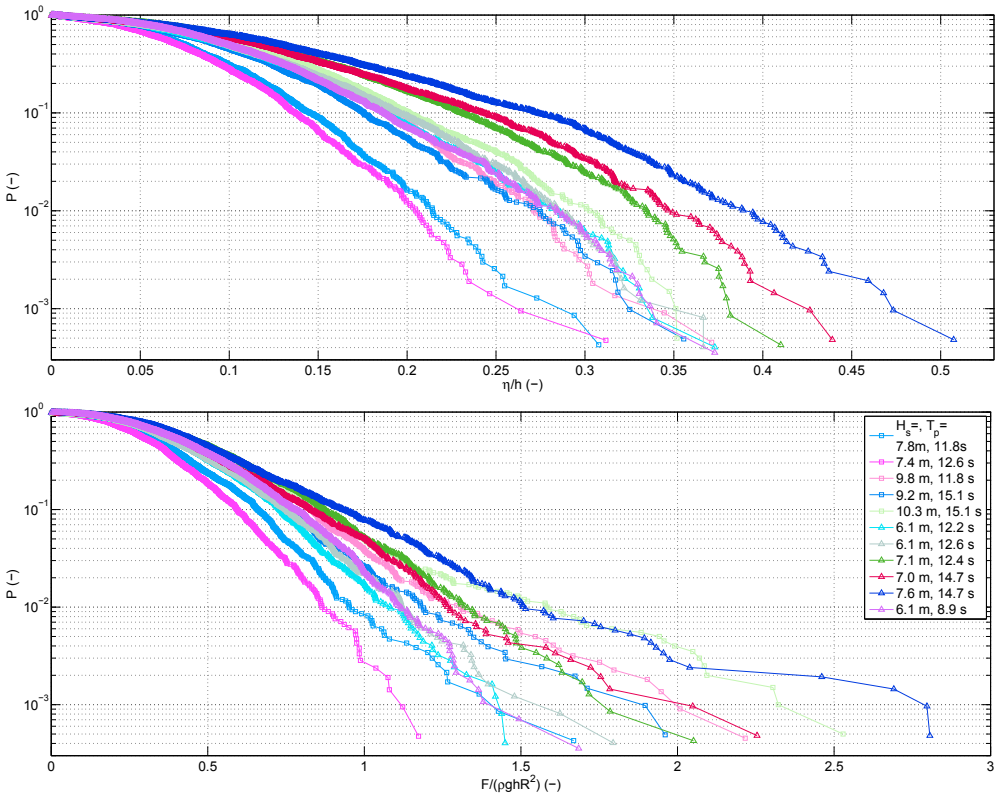

Fig. 4: Probability of exceedance of the crest heights and force peaks, when normalizing with h. □ h = 33m, △ h = 20m.

The standard deviations of the nine force shapes for each sea state are also shown. The variation is zero at $t = 0$ and increases away from the force peaks. However, from the zero-upcrossing in front of the peak to the through after the peak the nine forces show a strong similarity.

In figure 8 the average force shapes of the force peaks with the force value $F/(\rho g h R^2)$ =(0.8, 1.0, 1.2, 1.3, 1.6) are shown for all sea states. The force shapes are grouped after the values of $h/(gT_p)^2$ of their corresponding sea states, as shown in figure 2. The time is normalised with the scale T_a, which is the time from the force peak to the trough after the force peak of the linear NewForce signal for the same T_p-value. Thus, T_a is function of T_p and γ.

Below the force-shapes, the standard deviations of the average force shapes are shown. Generally, the shapes of the forces in each group match quite well and becomes more uniform as $F/(\rho g h R^2)$ increases.

The amplitude of the trough in front of the peak increases with increasing $h/(gT_p^2)$-value and decreases with increasing $F/(\rho g h R^2)$-value. In the analysis it was tried to find a time-scale which would give all forces the same nondimensional period. However, as seen in the figures, we did not manage to find such a time scale, and the time, t/T_a, from the peak to the trough after the peak increases with increasing $h/(gT_p^2)$. Still, we observe that the nondimensional time from the zero-upcrossing in front of the force peak to the through after the peak is almost identical for all forces for same $h/(gT_p^2)$-value when using this time normalization.

The secondary load cycle is seen for the smallest force-values $F/(\rho g h R^2) \geq 1.2$. It could look like the secondary load cycle force for $h/(gT_p^2)$ =0.009 occurs for smaller $F/(\rho g h R^2)$-values compared to the other $h/(gT_p^2)$-values. This illustrates, that nonlinearity increases with decreasing water depth.

Considering the standard deviation, the deviation decreases as $F/(\rho g h R^2)$ increases. The standard deviation is zero at $t = 0$ s, since all forces are normalized with their force peaks. The deviation increases on both sides of $t = 0$s to approximately the time of occurrence of the troughs, showing that the average forces are most uniform around the

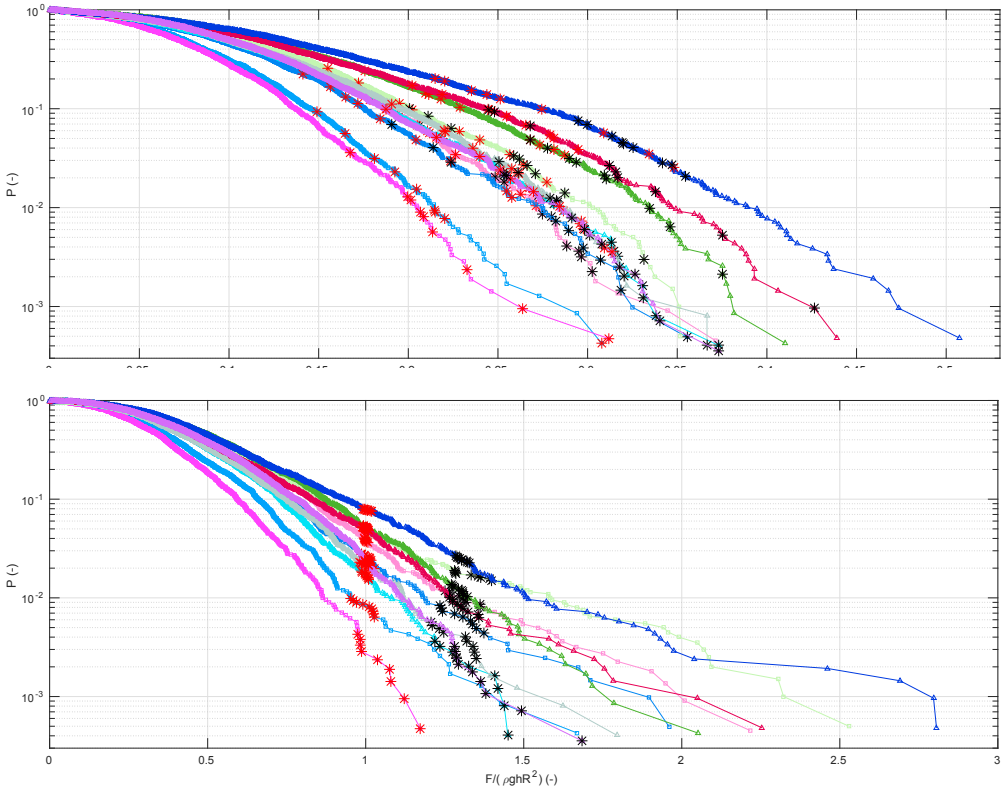

Fig. 5: Probability of exceedance of the crest heights and force peaks, when normalizing with h. □ h = 33m, △ h = 20m. The red and black asterisks shows the nine peak forces nearest the force values $F/(g\rho hR^2) = 1$ and $F/(g\rho hR^2) = 1.3$ and the corresponding crest values.

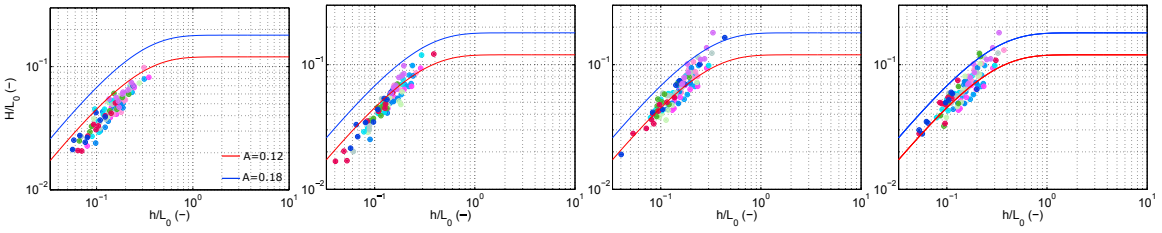

(a) $F/(g\rho hR^2) = 0.8$. (b) $F/(g\rho hR^2) = 1.0$. (c) $F/(g\rho hR^2) = 1.3$. (d) $F/(g\rho hR^2) = 1.6$.

Fig. 6: The breaking wave criteria of Goda [7]. The wave heights in the wave realizations corresponding to the 9 force peaks nearest the force values $F/(g\rho hR^2)$ for all 11 sea states.

force-crest. This is in accordance with the theory of NewWave, [17], where it is shown that as the crest height of the NewWave increases the standard deviation remains constant meaning that the surface elevation becomes more deterministic.

It is important to note that for smaller $F/(\rho ghR^2)$-values the standard deviation increases. The above observations indicating that the shapes of the normalized forces are a function of $h/(gT_p^2)$, t/T_a and $F/(\rho ghR^2)$ are therefore only good approximations for roughly $F/(\rho ghR^2) > 0.8$ in the present parameter range.

5.3. Comparison to the NewForce model

The NewForce model and the Morison equation are engineering tools, to calculate the wave forces. They are suited for application, as they are simple and easily calculated. In this section it is investigated how well the different

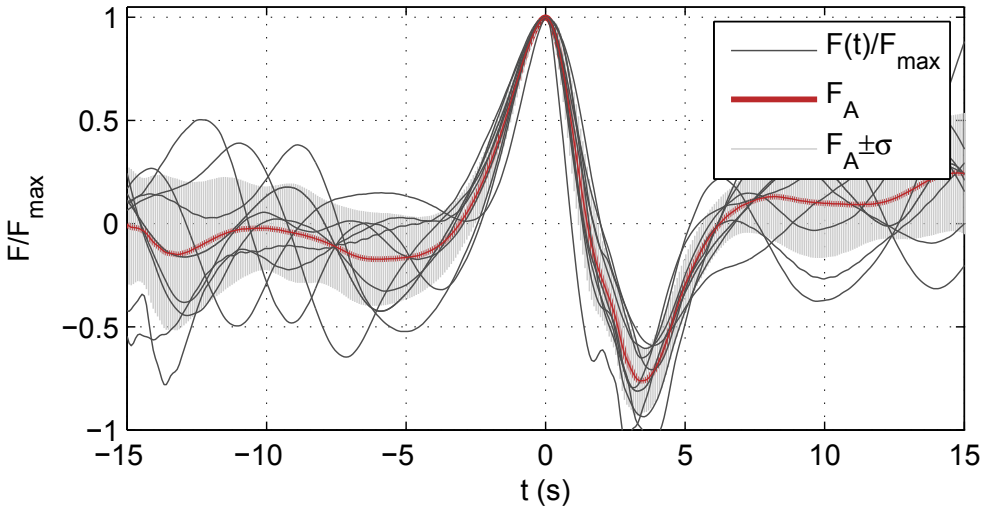

(a) $F/(\rho g h R^2) = 1.0$.

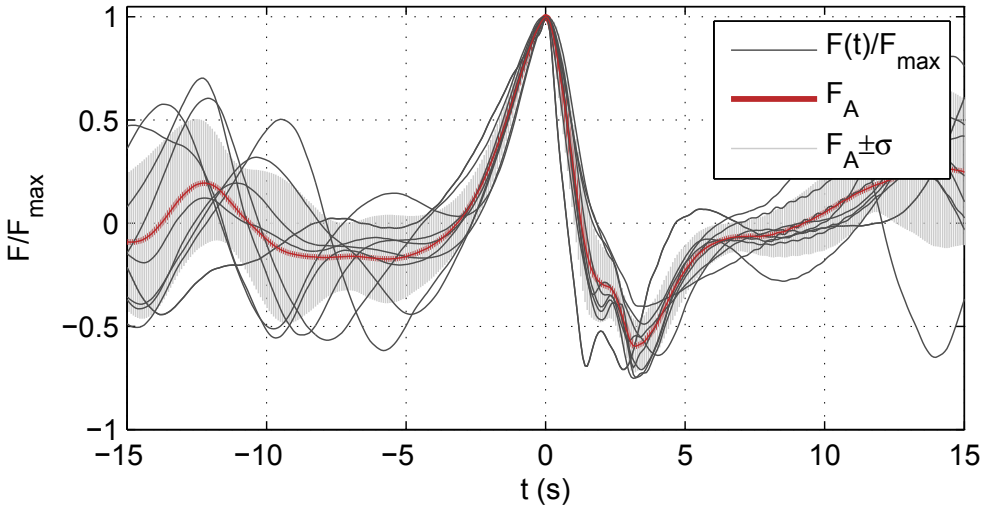

(b) $F/(\rho g h R^2) = 1.3$.

Fig. 7: The nine force shapes, $F(t)$, and the corresponding average force, F_A together with the standard deviation σ of the nine forces for the sea state with $H_s = 6.8$m, $T_p = 15$m and $h = 20$m.

force shapes presented in figure 8 can be predicted by the NewForce model extended to second order. The approach explained in section 3 is used to calculate the second order NewForce signals, $F^{(1)+(2)}_{\text{NewForce}} = F^{(1)}_{\text{NewForce}} + F^{(2)}_{\text{NewForce}}$.

Two examples with different $F/(\rho g h R^2)$-value are shown in figure 9 for the sea state with $H_s = 11$m, $T_p = 15$s and $h = 33$m. For comparison, the first and second order free surface elevations, η_{NewForce} based on the NewForce signals are also shown.

Since extreme sea states are considered, some of the average force-shapes includes slamming, which is easy to identify, as the force contains a ”hat” on top of the peak. This is seen in the average force in figure 9b. However, the wave slamming is not included in the NewForce model, and the slamming part of force-shape is therefore disregarded when compared to the NewForce signal. To account for this in the analysis, the average force shape around the crest is approximated by a fourth order polynomial, and the maximum value of this polynomial is instead used as target peak-value for the NewForce signal, α in (9).

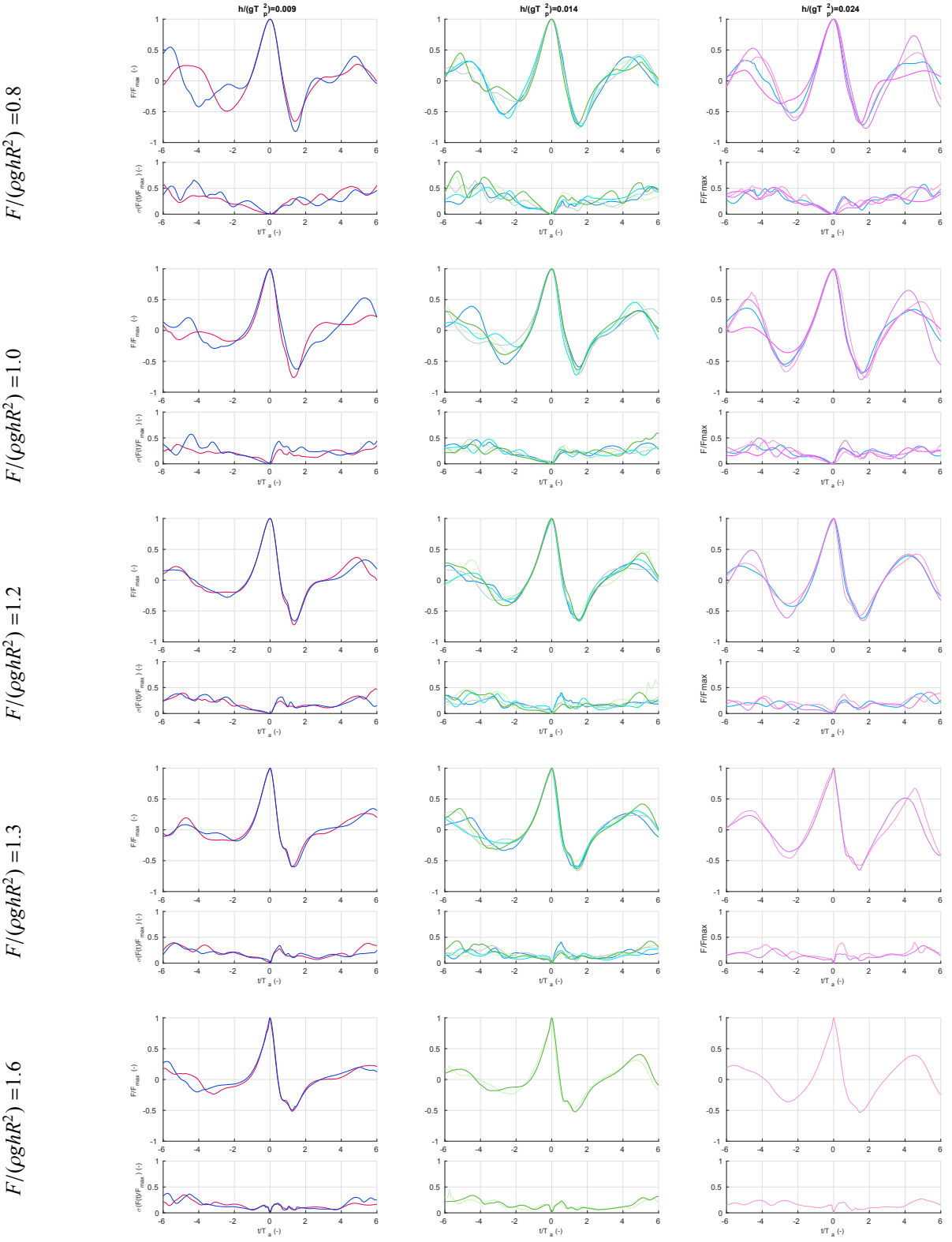

Fig. 8: The average force shape as function of $h/(gT_p^2)$ and $F/(\rho g h R^2$. The color of each sea state corresponds to the colors in figure 2.

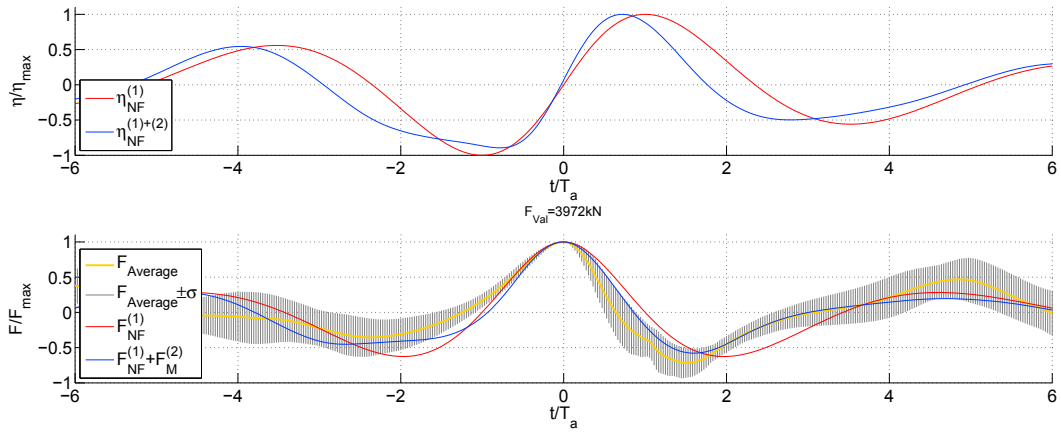

(a) $F/(\rho g h R^2) = 1.0$.

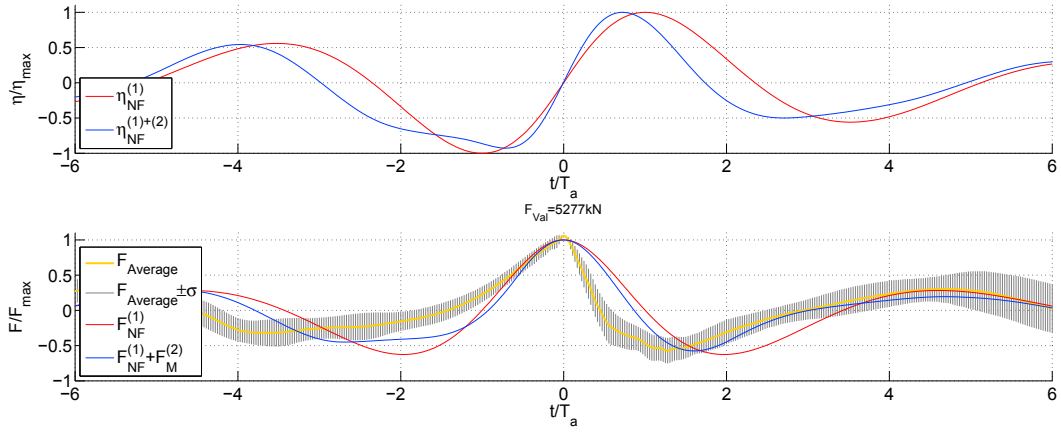

(b) $F/(\rho g h R^2) = 1.3$.

Fig. 9: The average force for the sea state with $H_s = 10.3$m, $T_p = 15.1$s, $h = 33$m and $h/(gT_p^2) = 0.014$ for two force values, and the corresponding NewForce signal and surface elevation based on the NewForce model.

Comparing the first and second order NewForce signals, the second order NewForce signal compares better to the average force signal. The trough in front of the peak is lifted upward and the force-crest becomes more narrow. This supports the finding that the time scale of the local force peak is not linear. It is therefore only the second order NewForce signal which is used in the following analysis. It is further seen that the NewForce signal and the average force compares best for the smallest force peak value, $F/(\rho g h R^2) = 1.0$, where the NewForce signal is inside the grey area indicating $F \pm \sigma$, with σ being the standard deviation. For $F/(\rho g h R^2) = 1.3$ the NewForce signal does not capture the asymmetry of the force shape, i.e. the force is more steep after the peak compared to in front of the peak. Higher-order terms are necessary to include such nonlinear effects.

The average force shapes of figure 8 are repeated in figure 10, but now they are compared to the corresponding second order NewForce signals. The NewForce signals for each $h/(gT_p)$ and $F/(\rho g h R^2)$ value are very similar and lie on top of each other for some situations. For the smallest force value, $F/(\rho g h R^2) = 0.8$, the NewForce signals compare very well to the average force shapes. However, as the force value increases, the differences between the average force shape and the NewForce signal increases. The dissimilarities are largest for the wave realizations in most shallow water, $h/(gT_p^2) = 0.009$ and occur for smaller force values compared to the two other groups of $h/(gT_p^2)$. This is a consequence of the stronger nonlinearity in shallow water, where accuracy of a second order model must decrease. The more shallow the more asymmetric the wave shapes become. The NewForce signal is more symmetric

around its crest value. This also explains why the crest of the NewForce signal is more steep in front of the peak compared to the average force, while after the peak, the average force is more steep.

The comparison indicates that it is possible to define limits based on $h/(gT_p)$ and $F/(\rho g h R^2)$, for which the expected force shape for a given sea state can be represented by the NewForce model extended to second order.

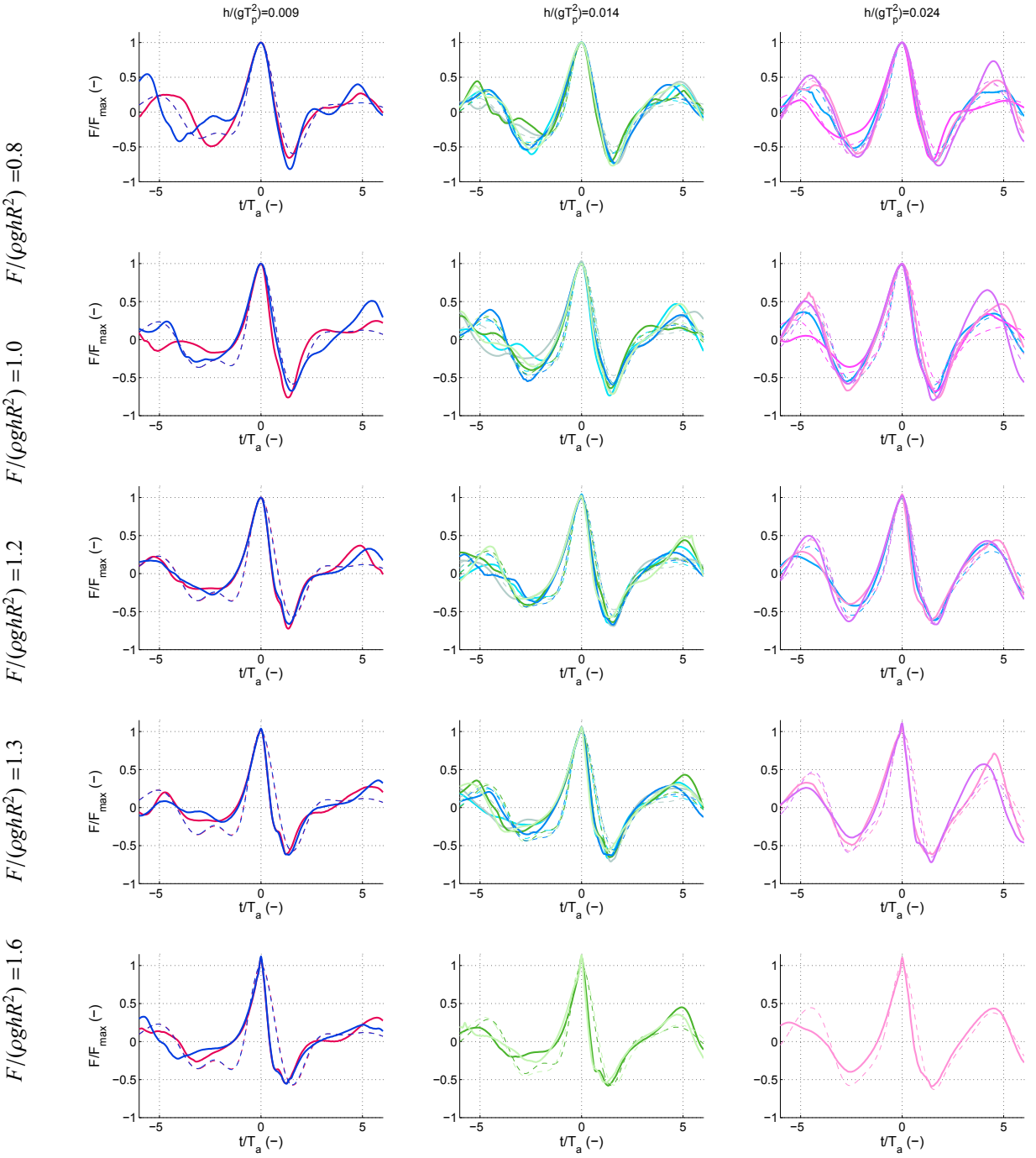

Fig. 10: The average force shape (full line) and the corresponding second force NewForce (dasped line) as function of $h/(gT_p^2)$ and $F/(\rho g h R^2$. The color of each sea state corresponds to the colors in figure 2.

6. Summary and discussion

Analysis of extreme wave forces based on experiments with a stiff pile has been presented. As the force-peaks are not only function of the wave height but also depends on e.g. the wave front slope, it is associated with uncertainties to base the design load on a design wave height only. The outset of the analysis was therefore to investigate if the force time history of extreme wave forces could be predicted directly based on force statistics, without having any information of the wave height and wave period resulting the specific force-value.

In the paper the NewForce model has been presented for the first time. In the NewForce model the NewWave theory principle is re-applied to obtain the expected force history around a force peak from the linear force spectrum.

The functional dependencies of the exceedance probability curves of the measured inline force and the normalised force shapes was investigated. It was found that the probability distributions of the force peaks are functions of both $H_s/(gT_p^2)$ and $h/(gT_p^2)$. For a given force value, the corresponding waves group around a curve parallel to the breaking limits of [7].

The normalised force shape was found to be function of $F/(\rho g h R^2)$, $h/(gT_p^2)$ and t/T_a with good similarity for $F/(\rho g h R^2) > 0.8$. Further, the second order NewForce model proved to predict the force shapes of moderate nonlinear waves well. The performance was found to be best for the larger values of $h/(gT_a^2)$, agreeing with the general decrease of nonlinearity towards larger depth. Thus, based on $h/(gT_p)$ and $F/(\rho g h R^2)$, limits can be defined, for which the expected force shape for a given sea state can be represented by second order NewForce model.

The presented analysis demonstrates that it is possible to estimate the exceedance probability curves of the force peaks and the associated force shapes from the normalised sea state parameters $H_s/(gT_p^2), h/(gT_p^2)$, and that the second-order NewForce model provides a good estimate of the expected force shape for waves of moderate nonlinearity. The extension to multidirectional wave realizations is straightforward and should be investigated in future work. While the present work addresses the linear expected event and adds the second-order terms, a direct determination of the most likely second-order event for a given force can be obtained by application of a First-Order Reliability Method (FORM). Such an investigation is presented by Ghadirian et al. [6] with comparison to the same data set and treatment of directional waves.

Slamming loads could be observed for the largest force levels as a distinct 'hat' on top of the smoother underlying force curve. While these seem beyond a simple slender-body force model, improved prediction of the force shapes of more nonlinear waves may be obtained by incorporating a wave model more accurate than second order. This could be the fully nonlinear wave model, OceanWave3D, [5] and is planned for future work.

Acknowledgment

DeRisk is funded by a research project grant from Innovation Fund Denmark, grant number 4106-00038B. Further funding is provided by Statoil and the participating partners. All funding is gratefully acknowledged.

DHI Denmark is thanked for providing the experimental data as part of the DeRisk-project. Simulating discussions with Prof. Paul Taylor, Dr. Thomas Adcock and Dr. Dripta Sarkar, University of Oxford, are acknowledged.

References

[1] Boccotti, P. (1983). Some new results on statistical properties of wind waves. *Applied Ocean Research 5*(3), 134–140.

[2] Bredmose, H., M. Dixen, A. Ghadirian, T. J. Larsen, S. Schløer, S. Andersen, S. Wang, H. Bingham, O. Lindberg, E. Christensen, et al. (2016). DeriskAccurate prediction of ULS wave loads. Outlook and first results. *Energy Procedia 94*, 379–387.

[3] Chen, M. (2011). Extreme wave-structure interaction and directional spreading effects on the air-gap design of an offshore platform. *WIT Transactions on The Built Environment 115*, 193–203.

[4] DNV-OS-J101 (2010, October). *Design of Offshore Wind Turbines*. Det Norske Veritas.

[5] Engsig-Karup, A., H. Bingham, and O. Lindberg (2009). An efficient flexible-order model for 3D nonlinear water waves. *Journal of Computational Physics 228*(6), 2100–2118.

[6] Ghadirian, A., H. Bredmose, and S. Schløer (2017). Prediction of the shape of inline wave force and free surface elevation using First Order Reliability method (FORM). In *DeepWind 2017*.

[7] Goda, Y. and T. Suzuki (1976). Estimation of incident and reflected waves in random wave experiments. *Coastal engineering proceedings 1*(15).

[8] Grice, J., P. Taylor, and R. Taylor (2015). Second-order statistics and cesigner waves for violent free-surface motion around multi-column structures. *Philosophical Transactions of the Royal Society of London A: Mathematical, Physical and Engineering Sciences 373*(2033), 20140113.

[9] IEC61400-3 (2009). *International Standard. Wind turbines Part 3: Design requirements for offshore wind turbines* (1 ed.).

[10] Jensen, J. J. (2005). Conditional second-order short-crested water waves applied to extreme wave episodes. *Journal of Fluid Mechanics 545*, 29–40.

[11] Lindgren, G. (1970). Some properties of a normal process near a local maximum. *The Annals of Mathematical Statistics*, 1870–1883.

[12] Paulsen, B. T., H. Bredmose, H. B. Bingham, and N. G. Jacobsen (2014). Forcing of a bottom-mounted circular cylinder by steep regular water waves at finite depth. *Journal of Fluid Mechanics 755*, 1–34.

[13] Rainey, R. (1989). A new equation for calculating wave loads on offshore structures. *Journal of Fluid Mechanics 204*, 295–324.

[14] Rainey, R. (1995). Slender-body expressions for the wave load on offshore structures. *Proceedings of the Royal Society of London. Series A: Mathematical and Physical Sciences 450*(1939), 391–416.

[15] Santo, H., P. Taylor, R. E. Taylor, and Y. Choo (2013). Average properties of the largest waves in hurricane camille. *Journal of Offshore Mechanics and Arctic Engineering 135*(1), 011602.

[16] Sharma, J. and R. Dean (1981). Second-order directional seas and associated wave forces. *Society of Petroleum Engineers Journal 21*(1).

[17] Tromans, P. S., A. R. Anaturk, P. Hagemeijer, et al. (1991). A new model for the kinematics of large ocean waves-application as a design wave. In *The First International Offshore and Polar Engineering Conference*. International Society of Offshore and Polar Engineers.

[18] Walker, D., P. Taylor, and R. E. Taylor (2004). The shapes of large surface waves on the open sea. In *Hydrodynamics VI: Theory and Applications: Proceedings of the 6th International Conference on Hydrodynamics, Perth, Western Australia, 24-26 November 2004*, pp. 309. CRC Press.

[19] Whittaker, C., A. Raby, C. Fitzgerald, and P. Taylor (2016). The average shape of large waves in the coastal zone. *Coastal Engineering 114*, 253–264.

[20] Williams, J. (1981). Limiting gravity waves in water of finite depth. *Philosophical Transactions of the Royal Society of London. Series A, Mathematical and Physical Sciences 302*, 139–188.